On Forward Model Uncertainty in EEG Source Localization

Stahlhut, Carsten; Mørup, Morten; Winther, Ole; Hansen, Lars Kai

Publication date:
2009

Document Version
Publisher's PDF, also known as Version of record

On Forward Model Uncertainty in EEG Source Localization

Carsten Stahlhut, Morten Mørup, Ole Winther, Lars Kai Hansen

Technical University of Denmark
Department of Informatics and Mathematical Modelling
Richard Petersens Plads, DK-2800 Kgs. Lyngby, Denmark

Technical report: 19th of January 2009, revised 4th of April 2011

Abstract

We give two quantitative contributions to electro-encephalography (EEG) source localization. First, we investigate how erroneous forward models influence current density source reconstruction. Second, we present the first unified hierarchical Bayesian framework that simultaneously reconstructs the sources and the forward model. Modeling the uncertainties involved in the forward model, i.e. the representation of the conductivity distribution, the cortical surface, and the electrode locations, has the potential of giving better source location.

1 Introduction

Electro-encephalography (EEG) holds great promise for functional brain imaging due to its high temporal resolution. In comparison with functional magnetic resonance imaging (fMRI) and positron emission tomography (PET), the slow hemodynamic response does not affect EEG. In addition fMRI and PET involve heavy scanner equipment and immobilization constraints that compromise the experimental situation, while EEG can be performed under much more natural conditions.

Today EEG based brain imaging suffers from a lack of spatial specificity due to the complex propagation of neural quasi-static electric fields to the array of sensors placed at the scalp surface. Motivated by the desire to perform reliable and precise reconstruction of the neural current density, much effort has been devoted to development of improved inversion methods. The current literature can be divided in two major approaches: Equivalent current dipole (ECD) and distributed models. In ECD methods [1, 2] it is assumed that the brain activity is generated by a small number of focal sources, which restricts the source localization problem to a challenge of determining the positions and orientations of the ECDs.

In distributed models several prior assumptions are made in order to solve the ill-posed inverse problem. For example l_2-norm approaches, like the weighted minimum norm method [3] and low resolution electromagnetic tomography (LORETA) [4], assume sources to be diffuse and highly distributed. On the other hand models based on the l_1-norm [5], l_p-norms [6], minimum variance beamformer [7], Bayesian model averaging [8], multiple priors models [9, 10], and automatic relevance determination methods [11], implement more focal sources. Most of these source localization methods employ spatial-temporal priors in order to accommodate for the focal source distribution.

While the existing literature concerns inversion under the assumption that the forward propagation model is known, we are interested in examining this assumption in more detail. *We give two quantitative contributions: We show that uncertainty of the forward model affects source localization, both when it derives from conductivity and geometrical uncertainty. Motivated by this observation we then devise the first hierarchical Bayesian model for simultaneous estimation of the current source density and the forward model. We show that the new model leads to improved source estimates.* Our Bayesian source localization approach with uncertain forward model is described in more details in [12].

The issue of modeling the forward process was recently approached from a different viewpoint in [13] where the basic structure of the forward model is assumed to be known, except for the different brain component's conductivity ratios. In the resulting parametric model two sources and the brain/skull conductivity ratio were estimated simultaneously. Here we take a much more uncommitted approach in which the whole forward process is considered uncertain within a hierarchical Bayesian framework. This approach is motivated by the many sources of uncertainty involved in formulating the forward model, including the representation of the conductivity distribution, the cortical surface, and the electrode locations. When medical imaging methods, e.g., tissue segmentation based on structural MRI, are used to construct a so-called 'realistic head model', resolution and tissue flexibility uncertainties affect the head geometry. These errors can be presented as small magnitude perturbations of the head model shape [14]. Besides the geometry of the head model, tissue conductivities also play a crucial role in determining the forward model. Due to the severe ill-posed nature of the EEG source reconstruction problem small perturbations in the head model, will affect the estimated sources.

This paper focuses on the role of the forward model, more specifically where in the brain can the current density be expected to be reliably reconstructed in the face of a given noise level? And how is this affected by an uncertain forward model? In a broader perspective this analysis may be used as guidance for which paradigms EEG can be used as a reliable functional imaging tool. Furthermore, the analysis motivates us to include the uncertainty of the head model into source reconstruction methods. We briefly present results of a hierarchical Bayesian model that integrates the uncertainty of the forward model.

2 Analysis of Forward Model Uncertainty

2.1 Forward Model

The first step in EEG source location is to formulate the forward model that determines the electromagnetic field from a specific set of sources, here assumed perpendicular to the cortex. This leads to a linear model of the form

$$\mathbf{M} = \mathbf{AS} + \mathbf{E}, \tag{1}$$

where $\mathbf{M}$ $(N_c \times N_t)$ represents the electric potentials at the scalp, $\mathbf{S}$ $(N_d \times N_t)$ the current sources over a time interval $(1 : N_t)$, and $\mathbf{E}$ is an additive noise term. $\mathbf{A}$ $(N_c \times N_d)$ is the forward model with columns $(\mathbf{a}_1, ..., \mathbf{a}_{N_d})$. The i^{th} column is the relationship between the i^{th} dipole and all the sensors. N_c, N_d, and N_t are the number of channels, sources (dipoles), and number of time samples, respectively. The so-called head model describes the geometry of the different conductivity components in the head. Different levels of complexity of the head model are described elsewhere, e.g. [15, 16]. The spherical head model, the boundary element method (BEM), and finite element methods (FEM) are examples of increasing complexity of the forward models. We use here a simple spherical head model consisting of 3-spheres (cortex, skull, and scalp). Several studies of the influence of the tissue conductivity have already been performed [17, 18, 19], with conductivity ratios between brain and skull in the range from 15 [20] to 80 [21].

2.2 Qualitative Analysis of the Role of Forward Model Uncertainty

In order to reveal the influence of the forward model on the reconstruction of the sources, we will evaluate how sources located in different regions of the brain are confused. We analyze a single time point, thus the linear model reads $\mathbf{m} = \mathbf{A}^*\mathbf{s}^* + \boldsymbol{\varepsilon}$, where '$*$' indicates the 'true' forward model and source distribution, respectively. We will assume that the true solution is sparse, i.e. only one source, say the i^{th}, is active with a strength s_i^*. When we infer the source signals we consider the quadratic cost function with a potentially incorrect forward model $\mathbf{A} \neq \mathbf{A}^*$,

$$E(\mathbf{s}) = \|\mathbf{m} - \mathbf{As}\|_2^2 \quad . \tag{2}$$

The sparse least squares (sls) estimate of a single dipole solution located at the site j is $s_j^{\text{sls}} = \mathbf{a}_j^T\mathbf{m}/|\mathbf{a}_j|^2$ and zero for all other components. Inserting this into the cost function and averaging over the noise distribution $\sigma_\varepsilon^2 = \left\langle \boldsymbol{\varepsilon}^T\boldsymbol{\varepsilon} \right\rangle / N_c$ we get the expected cost:

$$\langle E(j|i) \rangle = \left\langle \left\| \mathbf{m} - \mathbf{As}^{\text{sls}} \right\|_2^2 \right\rangle = |\mathbf{a}_i^* s_i^*|^2 \sin^2 v_{j,i} + N_c\sigma_\varepsilon^2 = |\mathbf{a}_i^* s_i^*|^2 \left(\sin^2 v_{j,i} + \frac{1}{\text{SNR}} \right) \tag{3}$$

with

$$\cos v_{j,i} = \frac{\mathbf{a}_j^T \mathbf{a}_i^*}{|\mathbf{a}_j||\mathbf{a}_i^*|}$$

and the signal-to-noise ratio (or inverse effective noise level) is defined as $\mathrm{SNR} = \frac{|\mathbf{a}_i^* s_i^*|^2}{N_c \sigma_\varepsilon^2}$. Thus even if we use the correct forward model $\mathbf{A} = \mathbf{A}^*$, hence $\sin v_{i,i} = 0$, the small signals from sulci and from cortical regions at larger distance from the sensors are more likely to be confused because the differences in angular factors $(\sin v_{j,i})^2$ can be small compared to the effective noise level. The geometrical nature of the confusion depends on the distribution of $\sin^2 v_{j,i}$ across the cortical surface. In the following we will inspect this distribution and the patterns of confusion it induces with and without uncertainty in the forward model. A more elaborate analysis based upon covariance of cost function differences will be pursued elsewhere.

The results in the analysis depend on both the cortical resolution and the electrode configuration. The dimension of $\mathbf{A}$ was set to (128×4004) and $\mathbf{A}^*$ to (128×7204), such that the true forward model has a higher cortical resolution. The forward fields were generated by the SPM5 academic software, which is freely available from `http://www.fil.ion.ucl.ac.uk/spm/`. The forward propagation is based on a 3-spheres model with conductivities $\rho_{\mathrm{brain}} = 0.33\mathrm{S/m}$, $\rho_{\mathrm{skull}} = 0.0041\mathrm{S/m}$, and $\rho_{\mathrm{scalp}} = 0.33\mathrm{S/m}$ corresponding to the ratios 1:1/80:1 as in [21].

In Fig.1 we first analyze the confusion in case of a correct forward model. Figure 1(b) illustrates the confusion of the different dipoles given the sources located in Fig.1(a). For the true dipole located in the left frontal lobe (Source 1) it is seen that dipoles close to the true dipole have low costs, hence, are likely to be selected in face of noise. This is a favorable situation in which a true source in this location will be confused mainly with nearby locations. However, if the true source is located in the temporal lope (Source 2), the confusion is amplified and distributed across large portions of cortex as seen in Fig.1(d). In the following we inspect the influence of using the ratios 1:1/80:1 (the 'correct' ratios in the simulations) with the ratios 1:1/15:1. There are many ways to summarize the distribution of confusion. Here we consider a source properly located if the identified source is within a certain range d of the true. We can quantify the decision process using the positive predictive value (PPV) (or precision [22]):

$$\mathrm{PPV} = \frac{\mathrm{TP}}{\mathrm{TP} + \mathrm{FP}}, \tag{4}$$

where we define the true positives (TP) as the locations where both $(\sin v_{j,i})^2 \leq 1/\mathrm{SNR}$ and the distance to the true dipole d_{ij} is smaller than threshold (d). A false positive (FP) is declared if $d_{ij} \geq d$. We map the distribution of PPV, and we will indicate by a white color the special cases when no occurrence of neither TP nor FP is found. In Fig.1(b) the noise variance is $\sigma_\varepsilon^2 = 220$, which corresponds to a signal-to-noise ratio $\mathrm{SNR} = 10$ for a typical source (mean of all $|a_i^*|^2$). Note that depending on the location of the true source we will have different effective SNRs. It is seen that with the given noise level a source located

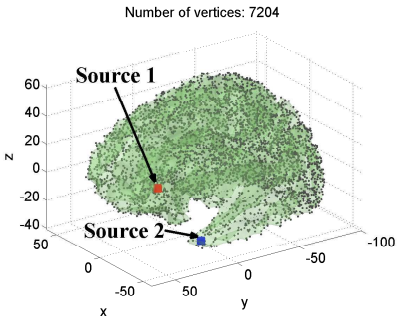

(a) Positions of two sources

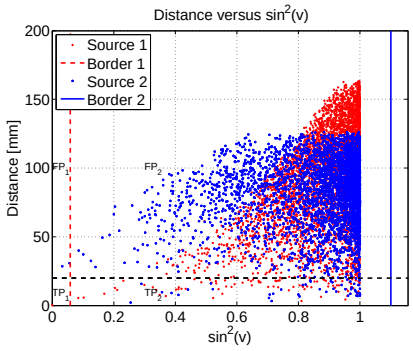

(b) Scatter plot of confusion

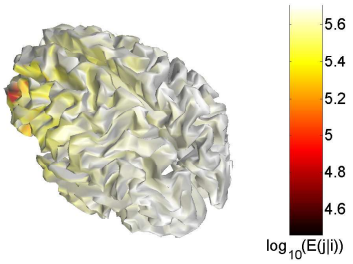

(c) Source 1: Error distribution

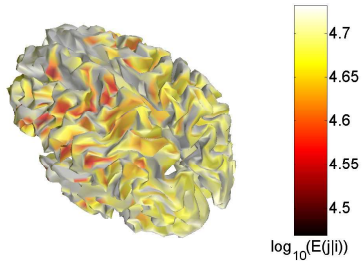

(d) Source 2: Error distribution

Figure 1: Comparison of the amount of expected confusion for two sources located in different cortical regions. (a) The positions of the two sources that are compared. Source 1 (left frontal part) and Source 2 (left temporal lope). (b) Scatter plots of the distance d_{ij} between the true source and each of the candidates (j^{th} dipole) versus angular factors $(\sin v_{j,i})^2$. The colors of the dots corresponds to their true source Source 1 & 2 in the top left plot. On the left side of Border 1 & 2 we have $(\sin v_{j,i})^2 \leq 1/\text{SNR}_1$ and $(\sin v_{j,i})^2 \leq 1/\text{SNR}_2$, respectively, where SNR_1 denotes the SNR when Source 1 is the true source and similar if we have Source 2. Likewise, subscript 1 and 2 for TP and FP are also related to the true sources Source 1 and Source 2. The threshold that separates TP and FP is $d = 20$mm. (c)+(d) The log error distribution illustrated on the cortex with Source 1 and Source 2 as the true source, respectively.

in the temporal lope (Source 2) is highly confused. In Fig.2 the true conductivities have been used. Figures 2(a) and 2(b) show the PPV distributions, while in Figs.2(c) and 2(d) we show worst case scenarios in two different views. In conclusion, the confusion of the reconstruction is very dependent on the location of the true source. It is well-known that sources located in sulci are generally more difficult to reconstruct in EEG compared to sources at gyri, since the ori-

entation of the sources from most of the sulcus areas is tangential, and we have seen here that these problems are further amplified when an incorrect forward models is applied.

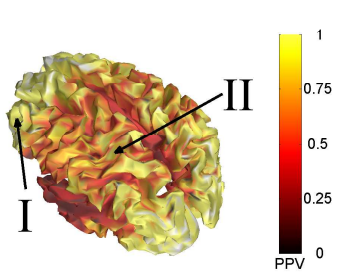

(a) Positive prediction values, view1

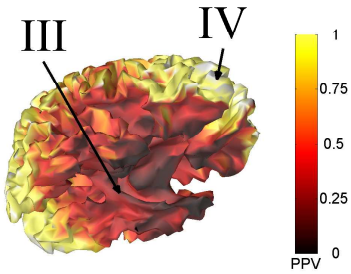

(b) Positive prediction values, view2

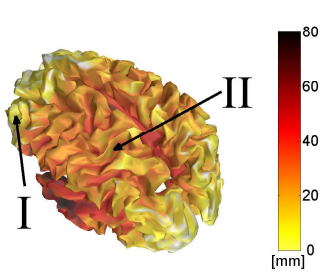

(c) Worst case loc. error, view1

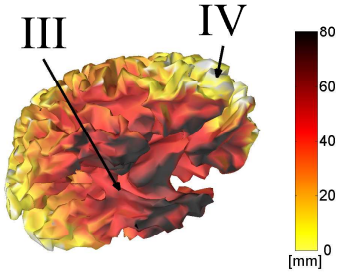

(d) Worst case loc. error, view2

Figure 2: Confusion measured in terms of PPVs and localization errors for the different parts of the cortex given the 'correct' conductivity ratios $\rho_{\text{brain}} : \rho_{\text{skull}} : \rho_{\text{scalp}} = 1 : 1/80 : 1$, $d = 20$mm, and $\sigma_\varepsilon^2 = 220$. The occipital and the frontal lope (region I) of the brain have quite high precision at the given noise level. In contrast the lower parts of the brain, like the temporal lope (region III), have much lower precision at the given noise level. Sources located in sulci are in general more confused than gyral sources (e.g., see region II).

A set of brain images for the case with brain:skull conductivity ratio 1:1/15 can be found in Fig.3, providing some insight in the role of conductivity uncertainty, c.f., Fig.2. Indeed a wrong conductivity ratio influences our ability to reconstruct sources correctly. Note the increase in areas where neither TP nor FP (region I+IV) have been found, which indicates an increase in the angular factors. In contrast to the case of reconstruction with a true brain:skull conductivity ratio (1:1/80) some areas like motor cortex, parietal region, and the lower part of the brain actually seems to be less confused when using the erroneous conductivity ratio 1:1/15! However, the angular factors also increase indicating

a poorer representation of the signal.

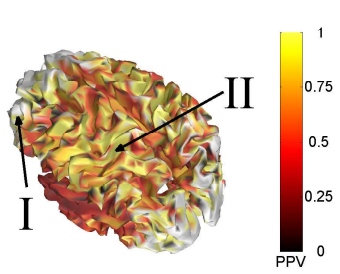

(a) Positive prediction values, view1

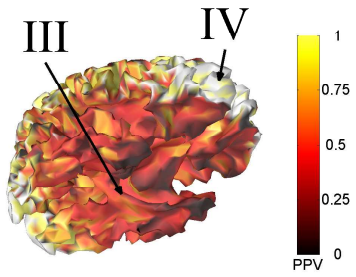

(b) Positive prediction values, view2

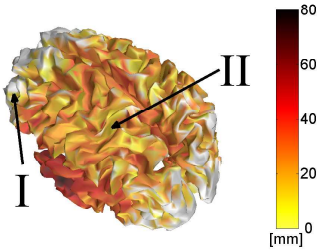

(c) Worst case loc. error, view1

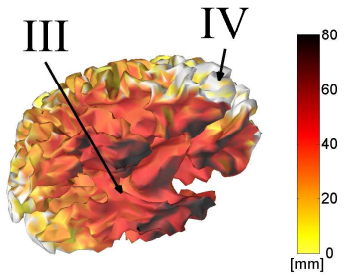

(d) Worst case loc. error, view2

Figure 3: PPVs and localization errors for the different parts of the cortex given the conductivity ratios $\rho_{\text{brain}} : \rho_{\text{skull}} : \rho_{\text{scalp}} = 1 : 1/15 : 1$, $d = 20$mm, and $\sigma_\varepsilon^2 = 220$. Increase in white areas where no TP or FP have been found (region I+IV) indicating increase in angular factors.

In Fig.4 a forward model with simple 'errors in the geometry' is analyzed. The errors are induced by scaling, rotating and translation of the cortex of the true model. Cortex has been scaled in the x, y, and z directions (see Fig.1(a)) with the factors 0.98, 0.95, and 0.92, respectively, and rotated around the x, y, and z-axis by -5, 5, and -5 degrees, respectively. Finally, a translation of 3mm, 3mm, and -2mm along the three coordinate directions was applied. The consequence of these errors in $\mathbf{A}$ is a general decrease in the PPV's and an increase in localization error especially for the upper part of the brain, e.g., the parietal lope, thus there are good reasons to attempt to heal such errors in the forward model.

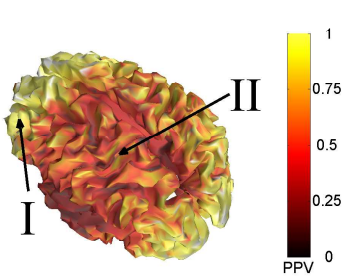

(a) Positive prediction values, view1

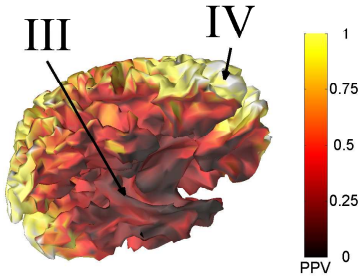

(b) Positive prediction values, view2

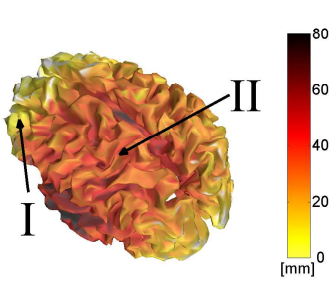

(c) Worst case loc. error, view1

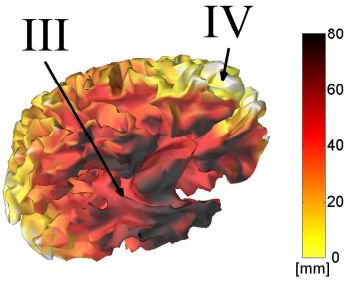

(d) Worst case loc. error, view2

Figure 4: PPVs and localization errors for the different parts of the cortex given the conductivity ratios $\rho_{\text{brain}} : \rho_{\text{skull}} : \rho_{\text{scalp}} = 1 : 1/80 : 1$, $d = 20\text{mm}$, $\sigma_\varepsilon^2 = 220$ and geometric errors.

3 Hierarchical Bayesian Approach to Joint Estimation of Source Density and Forward Model

In order to account for the uncertainty of the forward fields we use a hierarchical Bayesian model. A graphical representation of the model is given in Fig.5, where the noise is assumed zero-mean Gaussian distributed with precision β, i.e. $\mathbf{m}_t \sim \mathcal{N}\left(\mathbf{A}\mathbf{s}_t, \beta^{-1}\mathbf{I}\right)$. Similarly, the sources $\mathbf{s}_t$ are modeled as a zero-mean multivariate Gaussian distribution with precision matrix $\mathbf{D}$, $\mathbf{s}_t \sim \mathcal{N}\left(\mathbf{0}, \mathbf{D}^{-1}\right)$, where $\mathbf{D}$ is a diagonal matrix with the precision parameters $\boldsymbol{\alpha}$ in the diagonal. The uncertainty of $\mathbf{A}$ is modeled with each of the forward fields $\mathbf{a}_i$ as independent multivariate Gaussian, $\mathbf{a}_i \sim \mathcal{N}(\mathbf{a}_i^{(0)}, \gamma_i^{-1}\mathbf{I})$, where $\mathbf{a}_i^{(0)}$ is the prior mean for the i^{th} forward field. The assignment of a precision parameter to each of the columns in $\mathbf{A}$ allows us to reconstruct the forward fields for the most active sources, while the remaining forward fields will be forced to their prior means. All precision parameters are modeled with Gamma distributions with skewness

parameter $\boldsymbol{\nu}^x$ and inverse scale parameter $\boldsymbol{\zeta}^x$ as indicated in Fig.5. The model and its inference is described in more detail in [12].

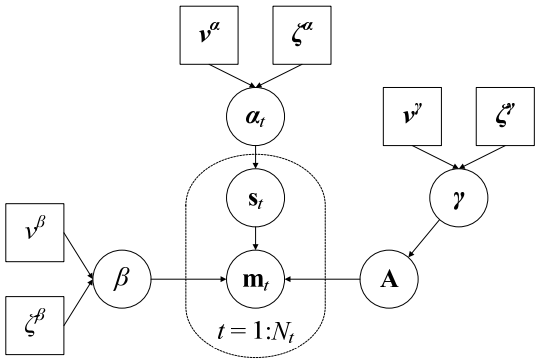

Figure 5: Graphical representation of hierarchical model that accounts for an uncertain forward model.

3.1 Simulation Experiment

We present the recovered source density estimates both with and without estimated forward fields. In the simulation a small area on the cortex in the left frontal hemisphere is simulated as active. The source signal consist of a half sine of duration 30ms starting at $t = 25$ms. The simulated sources at $t = 50$ms are shown in the SPM glass-brain representation in Fig.6(a). Due to the mapping from cortex to the glass-brain representation minor activity seems to appear at the inner part of left hemisphere. The corresponding simulated clean EEG is shown in Fig.6(b), while in Fig.6(c) we have corrupted the signal with 'realistic EEG noise' such that a SNR = 30 is obtained. The noise is adopted from an evoked EEG study [23], where we have used the pre-stimulus period as noise. In order to generate the noiseless EEG a 3-spheres head model with tissue conductivities brain:skull:scalp = 0.48:0.0019:0.48 $\frac{\mathrm{S}}{\mathrm{m}}$, corresponding to a ratio of 1:1/250:1, were used, and with a resolution of 7204 vertices.

In the source localization 3-spheres head models with dimensions of 4004 vertices are used. In the simulations we have only added conductivity errors. Figures 7(a)-(c) show the reconstructed sources at $t = 50$ms when no corrections of the forward fields are performed. The sources have been reconstructed with three different conductivity ratios. The true sources are generally quite good localized, however, a too small conductivity ratio as in Fig.7(a) compared to true ratio at 1:1/250:1 also causes detection of misleading activity in the right temporal lope. As the conductivity ratio approaches the true ratio the erroneous activity in the right temporal lope is reduced a bit. Note that the explained variance of the signal is 99.93 percent for the model with ratios 1:1/15:1 and 99.85 percent for the model with the true ratios 1:1/250:1, which indicate that noise is also fitted. From Fig.6(a) it is seen that the explained variance of the

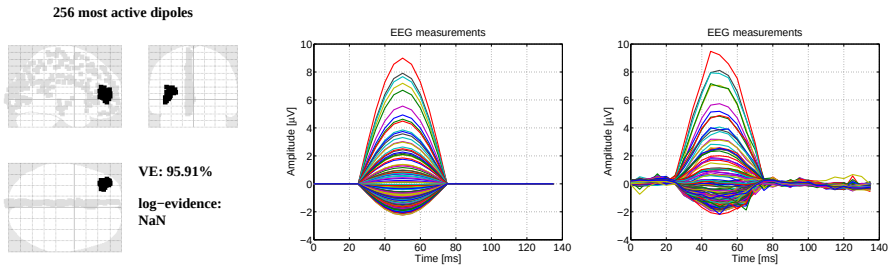

(a) True sources (b) Noiseless EEG (c) EEG with noise

Figure 6: (a) Simulated sources, VE: Variance explained. (b) EEG recordings without noise and based on a 3-spheres head model with tissue conductivities $\rho_{\text{brain}} = 0.48\frac{\text{S}}{\text{m}}$, $\rho_{\text{skull}} = 0.0019\frac{\text{S}}{\text{m}}$, and $\rho_{\text{scalp}} = 0.48\frac{\text{S}}{\text{m}}$. (c) EEG recordings with noise included.

signal should only be 95.91 percent. Furthermore, it is noted that the model with the true conductivity ratios in Fig.7(c) has the largest log-evidence indicating that this model is the most likely of the three in Figs.7(a)-(c). In Figs.7(d)-(f) the same forward models as in Figs.7(a)-(c) have been used as prior mean. We now apply the hierarchical model with the correction part for the erroneous forward fields. Indeed, all three cases lead to a minimization of the misleading activity in the right temporal lope that appeared for the results in Figs.7(a)-(c). The models with the three different starting conductivity ratios seem to lead to the same localization of the sources. The model with the true ratios 1:1/250:1 as prior mean seems to be more likely due to its large log-evidence. However, the explained variance for the model in Fig.7(f) is only 91.67 percent, which is a bit smaller than the expected at 95.91 percent. In contrast the model with a prior mean with ratios 1:1/15:1 obtains 95.48 percent explained variance, which is closer to the expected one. Since the explained variance for the model with the correcting part of the forward model all have explained variance values smaller than the expected this indicates that overfitting has been avoided.

4 Conclusion

We have given a qualitative analysis of the role of uncertainty in the forward model for the severe ill-posed EEG source reconstruction problem. Empirically, we have demonstrated how reconstructed sources may be expected to be confused with other sources in the brain, and how this effect is amplified by an erroneous forward model. Motivated by these unwanted effects of uncertain forward model, we presented the first results for a hierarchical Bayesian framework for simultaneous source localization and forward model estimation. Clearly, simultaneous source localization and forward model reconstruction makes the EEG source reconstruction even more ill-posed. However, the use of precision parameters on each of the forward field ensures that the forward model cor-

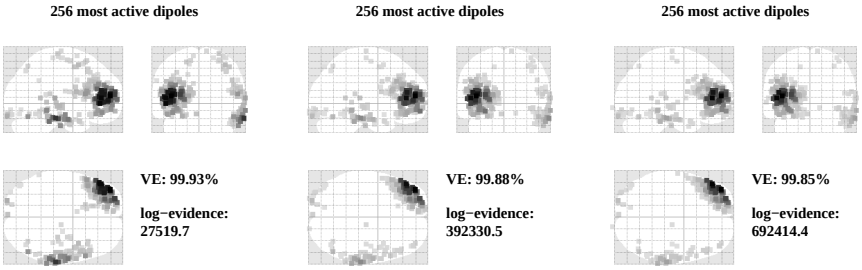

(a) Ratios 1:1/15:1 (b) Ratios 1:1/80:1 (c) Ratios 1:1/250:1

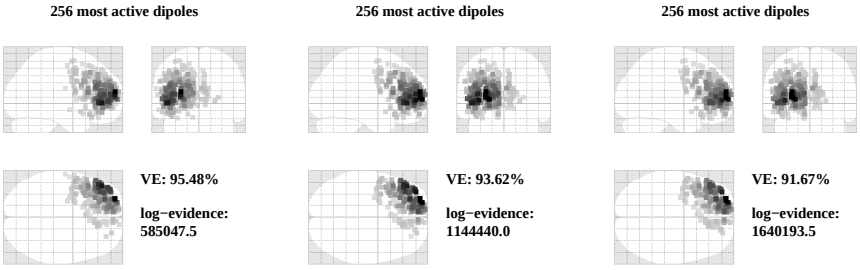

(d) Init ratios 1:1/15:1 (e) Init ratios 1:1/80:1 (f) Init ratios 1:1/250:1

Figure 7: Reconstructed activity at $t = 50$ms and weighted by the inverse variance $\boldsymbol{\alpha}$ when no corrections of forward fields are performed (first row) and when corrections is integrated into the source localization method (second row). Different conductivity ratios $\rho_{\text{brain}} : \rho_{\text{skull}} : \rho_{\text{scalp}}$ have been used as indicated in the images. VE: Variance explained.

rections mainly take place for the active dipoles. Simulations showed that the hierarchical Bayesian model accounting for forward model uncertainty was able to remove mis-located sources that we had found when no corrections of the forward fields were performed. In the present analysis we have used a 3-spheres head model, important future work will concern similar analyses with more realistic head models based on BEM and FEM.

References

[1] Mosher, J.C., Lewis, P.S., Leahy, R.M.: Multiple dipole modeling and localization from spatio-temporal MEG data. IEEE Trans. on Biomedical Engineering **39**(6) (1992) 541–557

[2] Scherg, M., Bast, T., Berg, P.: Multiple source analysis of interictal spikes: Goals, requirements, and clinical value. J. Clin. Neurophysiol. **16** (1999) 214–224

[3] Hämäläinen, M., Ilmoniemi, R.: Interpreting magnetic fields of the brain: minimum norm estimates. Med. Biol. Eng. Comput. **32** (1994) 35–42

[4] Pascual-Marqui, R., Michel, M., Lehmann, D.: Low resolution electromagnetic tomography: A new method for localizing electrical activity in the brain. Int J. Psychophys **18** (1994) 49–65

[5] Fuchs, M., Wagner, M., Kohler, T., Wischman, H.: Linear and nonlinear current density reconstructions. J. Clin. Neurophysiol. **16**(3) (1999) 267–295

[6] Auranen, T., Nummenmaa, A., Hämäläinen, M., Jääskeläinen, I., Lampinen, J., Vehtari, A., Sams, M.: Bayesian analysis of the neuromagnetic inverse problem with ℓ^p-norm priors. NeuroImage **26** (2005) 870–884

[7] Darvas, F., Pantazis, D., Yildrium, E.K., Leahy, R.: Mapping human brain function with MEG and EEG: methods and validation. NeuroImage **25** (2004) 383–394

[8] Trujillo-Barreto, N., Aubert-Vazquez, E., Valdes-Sosa, P.: Bayesian model averaging in EEG/MEG imaging. NeuroImage **21**(4) (2004) 1300–1319

[9] Mattout, J., Phillips, C., Penny, W., Rugg, M., Friston, K.: MEG source localization under multiple constraints: an extended Bayesian framework. NeuroImage **30**(3) (2006) 753–767

[10] Friston, K., Harrison, L., Daunizeau, J., Kiebel, S., Phillips, C., Trujillo-Barreto, N., Henson, R., Flandin, G., Mattout, J.: Multiple sparse priors for the M/EEG inverse problem. NeuroImage **39** (2008) 1104–1120

[11] Wipf, D., Ramrez, R., Palmer, J., Makeig, S., Rao, B.: Analysis of empirical bayesian methods for neuroelectromagnetic source localization. In Schölkopf, B., Platt, J., Hoffman, T., eds.: Advances in Neural Information Processing Systems 19. MIT Press, Cambridge, MA (2007) 1505–1512

[12] Stahlhut, C., Mørup, M., Winther, O., Hansen, L.K.: SOFOMORE: Combined EEG source and forward model reconstruction. In: Biomedical Imaging: From Nano to Macro, 2009. ISBI '09. IEEE International Symposium on. (282009-july1 2009) 450 –453

[13] Lew, S., Wolters, C., Anwander, A., Makeig, S., MacLeod, R.: Low resolution conductivity estimation to improve source localization. In: New Frontiers in Biomagnetism. Proc. of the 15th Int. Conf. on Biomag. Volume 1300 of Int. Congress Series. (2007) 149–152

[14] von Ellenrieder, N., Muravchik, C., Nehorai, A.: Effects of geometric head model perturbation on the EEG forward and inverse problems. IEEE Trans. Biomed. Eng. **53**(3) (March 2006) 421–429

[15] Mosher, J.C., Leahy, R.M., Lewis, P.S.: EEG and MEG: forward solutions for inverse methods. IEEE Transactions on Biomedical Engineering **46**(3) (1999) 245–259

[16] Ramon, C., Schimpf, P., Haueisen, J.: Influence of head models on EEG simulations and inverse source localizations. Biomed. Eng. Online **5**(10) (February 2006) 1–13

[17] Haueisen, J., Ramon, C., Eiselt, M., Brauer, H., Nowak, H.: Influence of tissue resistivities on neuromagnetic fields and electric potentials studied with a finite element model of the head. Biomedical Engineering, IEEE Transactions on **44**(8) (August 1997) 727–735

[18] Gencer, N., Acar, C.: Sensitivity of EEG and MEG measurements to tissue conductivity. Physics in Medicine and Biology **49**(5) (2004) 701–717

[19] Wolters, C., Anwander, A., Tricoche, X., Weinstein, D., Koch, M., MacLeod, R.: Influence of tissue conductivity anisotropy on EEG/MEG field and return current computation in a realistic head model: A simulation and visualization study using high-resolution finite element modeling. Neuroimage **30**(3) (2006) 813–826

[20] Oostendorp, T.F., Delbeke, J., Stegeman, D.F.: The conductivity of the human skull: results of in vivo and in vitro measurements. IEEE Transactions on Biomedical Engineering **47**(11) (2000) 1487–1492

[21] Homma, S., Musha, T., Nakajima, Y., Okamoto, Y., Blom, S., Flink, R., Hagbarth, K.E.: Conductivity ratios of the scalp-skull-brain head model in estimating equivalent dipole sources in human brain. Neuroscience Research **22**(1) (1995) 51–55

[22] Fawcett, T.: An introduction to ROC analysis. Pattern Recognition Letters **27**(8) (2006) 861–874

[23] Henson, R., Goshen-Gottstein, Y., Ganel, T., Otten, L., Quayle, A., Rugg, M.: Electrophysiological and hemodynamic correlates of face perception, recognition and priming. Cerebral Cortex **13** (2003) 793–805